

Title	Penetration of crustal melt beyond the Kunlun Fault into northern Tibet
Creators	Le Pape, Florian and Jones, Alan G. and Vozar, Jan and Wenbo, Wei
Date	2012
Citation	Le Pape, Florian and Jones, Alan G. and Vozar, Jan and Wenbo, Wei (2012) Penetration of crustal melt beyond the Kunlun Fault into northern Tibet. Nature Geoscience, 5 (5). pp. 330-335. ISSN 1752-0894 (Accepted Version)
URL	https://dair.dias.ie/id/eprint/1115/
DOI	http://dx.doi.org/10.1038/ngeo1449

Penetration of crustal melt beyond the Kunlun Fault into northern Tibet

Florian Le Pape^{1,2*}, Alan G. Jones¹, Jan Vozar¹ and Wei Wenbo³

Discerning the transition between the particularly weak Tibetan plateau lithosphere and its surrounding rigid blocks¹ is a key issue for complete understanding of the ongoing India-Eurasia collision. Geophysical studies²⁻⁵ and magmatic evidence^{6,7} support the notion that partial melt exists within the anomalously hot^{7,8} crust of northern Tibet. The Kunlun Fault, which accommodates the plateau eastward extrusion, has been identified as a significant rheological boundary⁴ between weak, warm Tibetan crust⁸ and the rigid Eastern Kunlun-Qaidam block. Magnetotellurics uses the natural variations of the Earth electromagnetic field and can detect the presence of interconnected melt phases. Herein we present reanalysed and remodelled magnetotelluric data from Phase III⁴ of the INDEPTH project. Our resistivity models were obtained using a new anisotropy code⁹ and highlight unequivocal evidence for anisotropy at the northern edge of the plateau. We suggest the anisotropic anomaly reveals transgressive penetrative intrusion of melt from the Tibetan crust to the north, weakening the crust beneath the Kunlun Shan, which compromises the prior Kunlun Fault identification as a major rheological boundary. As well as accommodating the north-south crustal shortening in Tibet, the crustal melt penetration is likely to characterize the growth of the plateau¹⁰ to the north.

The INDEPTH (International Deep Profiling of Tibet and Himalaya) Phase III 600-line magnetotelluric (MT) profile⁴ crosses three major northern Tibetan plateau tectonic complexes: the Qiangtang terrane, the Songpan-Ganzi terrane and the Eastern Kunlun-Qaidam terrane, respectively separated by the Jinsha River Suture (JRS) and the Kunlun Fault (KF) (Fig. 1). Although not remarkable at the surface, the JRS has been identified as a significant crustal boundary¹¹. The Songpan-Ganzi terrane is characterized by several kilometres of a thick sequence of Triassic turbidites¹². Those flysch complexes are mostly easily deformable pelites, deposited in a deep marine setting, which likely were underthrust to lower crustal depths in the Mesozoic and along Cenozoic thrust faults, such as the Fenghuo Shan-Nangqian, localizing Tertiary contractional deformation in central-northern Tibet¹². To the north, the 1,000 km long, east-west-trending Kunlun Fault follows the trace of the Anyimaqen-Kunlun-Muztagh suture separating the Songpan-Ganzi block from the Eastern Kunlun-Qaidam block¹². Just west of the Lhasa-Golmud highway, the fault splits into the South Kunlun Fault (SKF) and the Kunlun Fault (Fig. 1). In this study, a subset of 19 long period MT (LMT) stations and 34 broadband MT (BBMT) stations from the 1999 600-line survey (Fig. 1) are reanalysed and remodelled using modern techniques previously unavailable. Time series were not reprocessed⁴, but, at common locations, the BBMT and LMT data were remerged considering the LMT data as the shifting reference for statics control. The TE mode longer periods were not used from some sites (Supplementary Fig. 1) as they were more affected by noise and distortion due to the effect of the highly conductive Qaidam basin bounding the northern edge of the profile⁴. Previous inversions⁴ of the data from the 600-line used both MT modes (TM and TE) and vertical magnetic field data to derive highly-smoothed models that were all characterized by a relatively laterally-uniform, mid-crustal conductor extending from the south end of the 600-line profile to the Kunlun Shan

and ending abruptly at the Kunlun Fault. The high conductivity of the middle and lower crust south of the Kunlun Shan was interpreted as partial melt, consistent with prior interpretations of INDEPTH Phase II MT data further south^{5,13}. Our new 2D anisotropic resistivity model for the 600-line fits the data better (both in global RMS misfit and in local misfits) than the prior model, is more focussed, less "smooth", exhibits greater lateral variability and particularly highlights required electrical anisotropy in the north part of the profile (Fig. 2 and 3).

In this study, three models are highlighted: global anisotropic and isotropic models of the 600-line (Fig. 2) and a local anisotropic crustal model obtained using fewer stations and focusing on the upper to middle crust around the Kunlun Shan (Fig. 3). Strike analysis and distortion decomposition¹⁴ was applied to all data to determine the most appropriate 2D profile orientation perpendicular to geo-electric strike, and to correct the data for determinable galvanic effects. For all models, the geo-electric strike orientations were found to be in agreement with the east-west trend of the main geological structures. The models were obtained using a modified version of a 2D MT inversion algorithm¹⁵ incorporating a trade-off parameter for electrical anisotropy⁹. The 2D anisotropy problem is restrictively solved by assuming that the anisotropy axes are parallel and perpendicular to the main axis of regional geo-electric strike, an assumption valid for this region but not generally applicable. Anisotropic modelling defines three models; xx - horizontal resistivity across profile, yy - horizontal resistivity along profile, and zz - vertical resistivity (the zz model is not shown as it is very similar to xx). The data were inverted simultaneously for both TM and TE modes and also the vertical magnetic field (Hz) transfer function (Supplementary Figs. 1 and 2).

Both isotropic and anisotropic models are consistent on a lithospheric scale and exhibit several robust features that were not evident in the previous isotropic solutions⁴, but show significant differences in the middle-lower crust of the Kunlun Shan area. First of all, on both global and focused inversions the anisotropic modelling particularly highlights an extension of the conductive anomaly to the north in the y direction (Figs. 2 and 3), i.e., the profile direction perpendicular to the fault. Secondly, vertical offsets in the mid-crustal conductive layer south of the SKF show convincing spatial correlations with locally-mapped tectonic features (Fig. 2). Furthermore, from the resistivity constraints inferred by our new model (Supplementary Fig. 3), the upper mantle is not as conductive as the crust, suggesting that the upper mantle cannot contain as great a volume of interconnected melt. Finally, north of the SKF, the crust and upper mantle are far more resistive and must be characterized by colder temperatures, and therefore stiffer rheological conditions. Furthermore, in the southern edge of the profile, the deeper part of the mantle (>100 km depth) is relatively resistive (Fig. 2). As the crustal conductor can reduce resolution of deeper structures, the resistivity imaged by the MT model is a minimum bound¹⁶ and the true resistivity of this particular feature is likely to be higher. However, due to the presence of the strong crustal conductors, the deep mantle structure in the middle of the profile is not well resolved (Supplementary Fig. 3).

The partial melt characterized by high conductivity in the Qiangtang and Songpan-Ganzi crust will follow surface magmatism variations in both space and time. Eocene to Oligocene magmatism in the Qiangtang Terrane is mainly associated with reactivation of the Mesozoic Bangong and Jinsha sutures, with northward subduction of Lhasa terrane and southward subduction of Songpan-Ganzi terrane respectively⁶. Middle Miocene to Quaternary magmatism,

although minor, is widely distributed in the Songpan-Ganzi terrane, and more locally in the northern Qiangtang terrane⁶. The conductivity of a partially molten rock depends on interconnectivity of melt, as opposed to melt insulated in pockets, and melt interconnectivity exists at low melt fractions¹⁷. Large volume fractions of melt are not required to explain our MT model, however our model highlights and reconfirms that melt is widespread in the crust, as proposed previously⁵. The recent volcanism in northern Tibet, as well as the widespread crustal melting (Fig. 2), is likely to be the consequence of the southward subduction of Asian lithospheric mantle beneath the Songpan-Ganzi terrane, imaged by seismic receiver functions¹⁸, associated with convective thinning of the Tibetan mantle lithosphere^{7,18,19}. The latter explains the widespread distribution of potassic volcanism in the Songpan-Ganzi terrane^{6,7}. Our model highlights resistive mantle at 140 km in the south of the profile, which does not agree with thin Tibetan lithosphere extending further south of the Bangong–Nujiang Suture zone¹⁸. The resistive feature is too resistive to corroborate the thin Tibetan Plate¹⁸ but not deep enough to be the Asian Plate¹⁸. Its interpretation remains enigmatic.

The crustal conductivity structure in our model exhibits marked vertical offsets beneath the surface traces of the Tanggula Thrust System (TTS) and the Jinsha River Suture (Fig. 2). Lateral variation in conductivity observed in the conductive layer can be due to changes in porosity within the layer, in layer thickness, in the degree of melting, and in the degree of interconnectivity of the melt phase²⁰. Surface elevation homogeneity across the Jinsha suture, in contrast to observed irregular Moho geometry^{11,21}, is explained by weak middle-lower crust, mapped by the MT model, that decouples crust-mantle boundary deformation. This decoupling is characterized by the offset observed in the conductive layer across the suture (Fig. 2). North of

the Tanggula Shan, a similar behaviour is observed across the TTS. During the Eocene, the TTS may have played a major role in the uplift of the early Tibetan plateau²², in association with the reactivation of the Jinsha suture²³. The Tibetan plateau likely grew through major thrust systems such as the TTS²², with the modern equivalent being the North Kunlun Thrust (NKT) (Fig. 1) bounding the northern edge of the plateau with a major drop in elevation. The decoupling of the deformation, generated by the presence of a weak middle lower crust, associated with the step-by-step thickening of the crust²¹, likely contributed to the atypical topography of the plateau.

In order to test the anisotropic feature observed on our new 600-line 2D anisotropic inversion model (Figs. 2 and 3), 3D synthetic modelling²⁴ (Fig. 4) was undertaken to study systematically MT sensitivity to the 3D resistivity transition between the Songpan-Ganzi and the more resistive Eastern Kunlun-Qaidam block. The presence of melt was modelled by adding a conductive layer in the middle crust. Different types of 3D melt intrusion penetrating into the most resistive block are simulated (Fig. 4) to account for the anisotropic feature observed in the new models. The anisotropic inversion⁹ was applied on the synthetic forward responses generated by the 3D models (Fig. 4). The inversion results show that our 600-line observations are more likely to be corroborating an anisotropic feature characterized by finger-shaped melt intrusions in contrast to a single intrusion. However, the width, thickness and deviations in the orientation of those finger-shaped intrusions cannot be resolved at the observed depths.

Our anisotropic modelling highlights a transgressive, penetrative-extension of the mid-crustal conductive anomaly to the north, crossing the upper crustal sharp resistivity contrast characterizing the subvertical Kunlun Fault (Fig. 3). Furthermore, the crustal model shows that

the anisotropic structure is consistent with wide-angle seismic data²⁵ (Fig. 3). According to our 3D synthetic modelling (Fig. 4), the anisotropic conductive anomaly is likely to be a finger-like manner intrusion of melt beneath the Kunlun Shan. These melt intrusions in the Kunlun middle crust may have been triggered by strain heating²⁶. The weak middle crust crossing the Kunlun Fault is likely to be locally decoupling the upper crust deformations from the lower crust and mantle. In partially molten rocks, the strength of the rock is mainly controlled by the degree of interconnection of melt. Therefore, as the greatest strength drop occurs for low melt fractions ($< 7\%$)²⁷, low melt fractions have a significant effect on rock rheology. This shows that low melt intrusions would be sufficient to change the rheology of the Kunlun crust. The weaker Kunlun crust thickens vertically in response to the crustal shortening between India and the more rigid Asian blocks represented here by the Qaidam basin, leading to a Moho offset at the Kunlun-Qaidam border²⁸. The finger-like penetrative melt extension to the north, weakening the Kunlun crust, stops at this offset at this time²⁵. However, the anisotropy anomaly may not be homogeneous along the whole of the northern Tibetan border, and its depth and horizontal extension to the north will likely vary. In addition to the eastward crustal flow in eastern Tibet²⁹ characterizing the east-west extension of the plateau, the melt penetration across the Kunlun Fault is accommodating crustal shortening in northern Tibet but may also characterize the growth of the plateau¹⁰ to the north, with extension of the crustal thickening to the south of the Qaidam basin²⁵.

Methods

The 2D MT isotropic modelling approximation assumes that resistivity does not vary perpendicularly to the profile direction. However, the profile orientation defined by the stations

positions is not necessarily in the correct orientation for this 2D approximation. Furthermore, galvanic distortion effects associated with local 3D inhomogeneities need to be removed also. The strike analysis or distortion decomposition was then applied to all stations and frequencies simultaneously in order to obtain a robust estimation of the regional geo-electric strike and remove the galvanic distortion effects due to local 3D structures¹⁴. Once the geo-electric strike is estimated, the data are rotated according to the strike direction and the stations are projected on a profile perpendicular to the strike orientation. The along-strike currents characterize the 2D TE-mode and the vertical magnetic field response functions, and across strike currents are associated with the 2D TM-mode. As the geo-electric strike is characteristic of the global orientation of the 2D regional structures from the upper crust down to the upper mantle, it may differ from the geology strike observed at the surface. Our strike analyses led us to adopt N85°E as the global profile (Fig. 2) geo-electric strike and N75°E as the focused profile (Fig. 3) geo-electric strike, which is in agreement with the east-west trend of the main geological structures.

The 2D anisotropic approximation⁹ works similarly to the 2D isotropic approximation, but assumes the conductivity varies along anisotropy axes defined as parallel and perpendicular to the main axis of the regional geo-electric strike. The anisotropic inversion code seeks suitable models with an imposed regularization constraint on the closeness of the three models in the three directions⁹ (xx - horizontal resistivity across profile, yy - horizontal resistivity along profile, and zz - vertical resistivity). For isotropic inversion, the closeness is set to a high value (100000) resulting in three models that are identical. For all anisotropic models, the models closeness used was 1, except a value of 0.3 was used for the anisotropic crustal model. Furthermore, for the global and crustal models, the error floors of 8%-3% and 10%-3% were respectively applied for

TM and TE apparent resistivity and phase, as well as 0.1 for the Hz transfer function for the inversions. The smoothness trade-off lambda used was 1.

References

1. Jordan, T. A. & Watts, A. B. Gravity anomalies, flexure and the elastic thickness structure of the India-Eurasia collisional system. *Earth Planet. Sci. Lett.* **236**, 732-750 (2005).
2. Fan, G. W. & Lay, T. Strong Lg wave attenuation in the Northern and Eastern Tibetan Plateau measured by a two-station/two-event stacking method. *Geophys. Res. Lett.* **30**, 1530 (2003).
3. Owens, T. J. & Zandt, G. Implications of crustal property variations for models of Tibetan plateau evolution. *Nature* **387**, 37-43 (1997).
4. Unsworth, M. *et al.* Crustal and upper mantle structure of northern Tibet imaged with magnetotelluric data. *J. Geophys. Res.* **109**, B02403 (2004).
5. Wei, W. *et al.* Detection of Widespread Fluids in the Tibetan Crust by Magnetotelluric Studies. *Science* **292**, 716-719 (2001).
6. Ding, L., Kapp, P., Zhong, D. L. & Deng, W. M. Cenozoic Volcanism in Tibet: Evidence for a Transition from Oceanic to Continental Subduction. *J. Petrol.* **44**, 1833-1865 (2003).
7. Chung, S. L. *et al.* Tibetan tectonic evolution inferred from spatial and temporal variations in post-collisional magmatism. *Earth-Science Rev.* **68**, 173-196 (2005).
8. Klemperer, S. L. in *Channel Flow, Ductile Extrusion and Exhumation in Continental Collision Zones* Vol. 268 (eds Law, R. D., Searle, M. P. & Godin, L.) 39-70 (Geological Society, Special Publications, 2006).

- 204 9. Baba, K., Chave, A. D., Evans, R.L., Hirth, G. & Mackie, R. L. Mantle dynamics beneath the
205 East Pacific Rise at 17°S: Insights from the Mantle Electromagnetic and Tomography
206 (MELT) experiment. *J. Geophys. Res.* **111**, B02101 (2006).
- 207 10. Medvedev, S. & Beaumont, C. in *Channel Flow, Ductile Extrusion and Exhumation in*
208 *Continental Collision Zones* Vol. 268 (eds Law, R. D., Searle, M. P. & Godin, L.) 147-164
209 (Geological Society, Special Publications, 2006).
- 210 11. Wittlinger, G. *et al.* Seismic tomography of northern Tibet and Kunlun: Evidence for crustal
211 blocks and mantle velocity contrasts. *Earth Planet. Sci. Lett.* **139**, 263-279 (1996).
- 212 12. Yin, A. & Harrison, T. M. Geologic Evolution of the Himalayan-Tibetan Orogen. *Annu. Rev.*
213 *Earth Planet. Sci.* **28**, 211-280 (2000).
- 214 13. Chen, L. *et al.* Electrically Conductive Crust in Southern Tibet from INDEPTH
215 Magnetotelluric Surveying. *Science* **274**, 1694-1696 (1996).
- 216 14. McNeice, G. W. & Jones, A. G. Multisite, multifrequency tensor decomposition of
217 magnetotelluric data. *Geophysics* **66**, 158-173 (2001).
- 218 15. Rodi, W. & Mackie, R. L. Nonlinear conjugate gradients algorithm for 2-D magnetotelluric
219 inversion. *Geophysics* **66**, 174-187 (2001).
- 220 16. Jones, A. G. Imaging the continental upper mantle using electromagnetic methods. *Lithos* **48**,
221 57-80 (1999).
- 222 17. Partzsch, G. M., Schilling, F. R. & Arndt, J. The influence of partial melting on the electrical
223 behavior of crustal rocks: laboratory examinations, model calculations and geological
224 interpretations. *Tectonophysics* **317**, 189-203 (2000).
- 225 18. Zhao, W. *et al.* Tibetan plate overriding the Asian plate in central and northern Tibet. *Nature*
226 *Geosci.* **4**, 870–873 (2011).

- 227 19. Arnaud, N. O., Vidal, P., Tapponnier, P., Matte, P. & Deng, W. M. The high K₂O volcanism
228 of northwestern Tibet: Geochemistry and tectonic implications. *Earth Planet. Sci. Lett.* **111**,
229 351-367 (1992).
- 230 20. Li, S. *et al.* Partial melt or aqueous fluids in the mid-crust of Southern Tibet? Constraints
231 from INDEPTH magnetotelluric data. *Geophys. J. Int.* **153**, 289-304 (2003).
- 232 21. Vergne, J. *et al.* Seismic evidence for stepwise thickening of the crust across the NE Tibetan
233 plateau. *Earth Planet. Sci. Lett.* **203**, 25-33 (2002).
- 234 22. Wang, C. *et al.* Constraints on the early uplift history of the Tibetan Plateau. *P. Natl. Acad.*
235 *Sci. USA.* **105**, 4987-4992 (2008).
- 236 23. Roger, F. *et al.* An Eocene magmatic belt across central Tibet: mantle subduction triggered by
237 the Indian collision? *Terra Nova* **12**, 102-108 (2000).
- 238 24. Mackie, R. L., Smith, J. T. & Madden, T. R. Three-dimensional electromagnetic modeling
239 using finite difference equations: The magnetotelluric example. *Radio Sci.* **29**, 923-935
240 (1994).
- 241 25. Karplus, M. S. *et al.* Injection of Tibetan crust beneath the south Qaidam Basin: Evidence
242 from INDEPTH IV wide-angle seismic data. *J. Geophys. Res.* **116**, B07301 (2011).
- 243 26. Whittington, A. G., Hofmeister, A. M. & Nabelek, P. I. Temperature-dependent thermal
244 diffusivity of the Earth's crust and implications for magmatism. *Nature* **458**, 319-321 (2009).
- 245 27. Rosenberg, C. L. & Handy, M. R. Experimental deformation of partially melted granite
246 revisited: implications for the continental crust. *J. Metamorph. Geol.*, **23**, 19-28 (2005).
- 247 28. Shi, D., Shen, Y., Zhao, W. & Li, A. Seismic evidence for a Moho offset and south-directed
248 thrust at the easternmost Qaidam-Kunlun boundary in the Northeast Tibetan plateau. *Earth*
249 *Planet. Sci. Lett.* **288**, 329-334 (2009).

29. Bai, D. *et al.*, Crustal deformation of the eastern Tibetan plateau revealed by magnetotelluric imaging. *Nature Geosci.* **3**, 358 - 362 (2010).
30. Jones, A. G. On the Equivalence of the "Niblett" and "Bostick" Transformations in the Magnetotelluric Method. *J. Geophys.* **53**, 72-73 (1983).

Contact Information

¹Dublin Institute for Advanced Studies, 5 Merrion Square, Dublin, Ireland

²National University of Ireland Galway, University Road, Galway, Ireland

³China University of Geosciences Beijing, 29 Xueyuan Road, Beijing, 100083, China

*email: flepape@cp.dias.ie

Acknowledgements

We would like to thank Science Foundation of Ireland (SFI) for the financial support (Grants 08/RFP/GEO1693 "INDEPTH4" and 07/RFP/GEOF759 "Anisotropy of the Continental Lithosphere" to AGJ) and Martyn Unsworth and the other members of the INDEPTH MT team from China, U.S.A., Canada and Ireland.

Author Contributions

F. Le Pape re-analyzed, modelled and interpreted the data and wrote the paper. A. G. Jones interpreted the data and wrote the paper. J. Vozar interpreted the data. W. Wei designed the project.

Competing Financial Interests statement

The authors declare no competing financial interests.

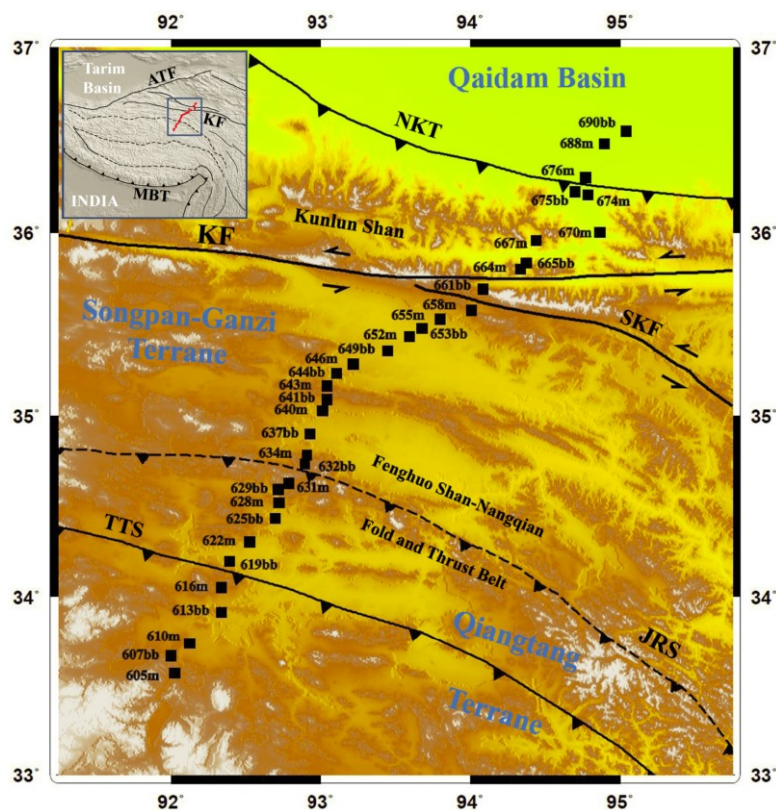


Figure 1. Location of the 600-line MT stations associated with the regional tectonic settings.

The map shows the locations of the long period and broadband merged stations (m) as well as broadband only stations (bb). ATF – Altyn Tagh Fault, KF - Kunlun Fault, MBT – Main Boundary Thrust, NKT - North Kunlun Thrust, SKF - South Kunlun Fault, JRS – Jinsha River Suture, TTS - Tanggula Thrust System.

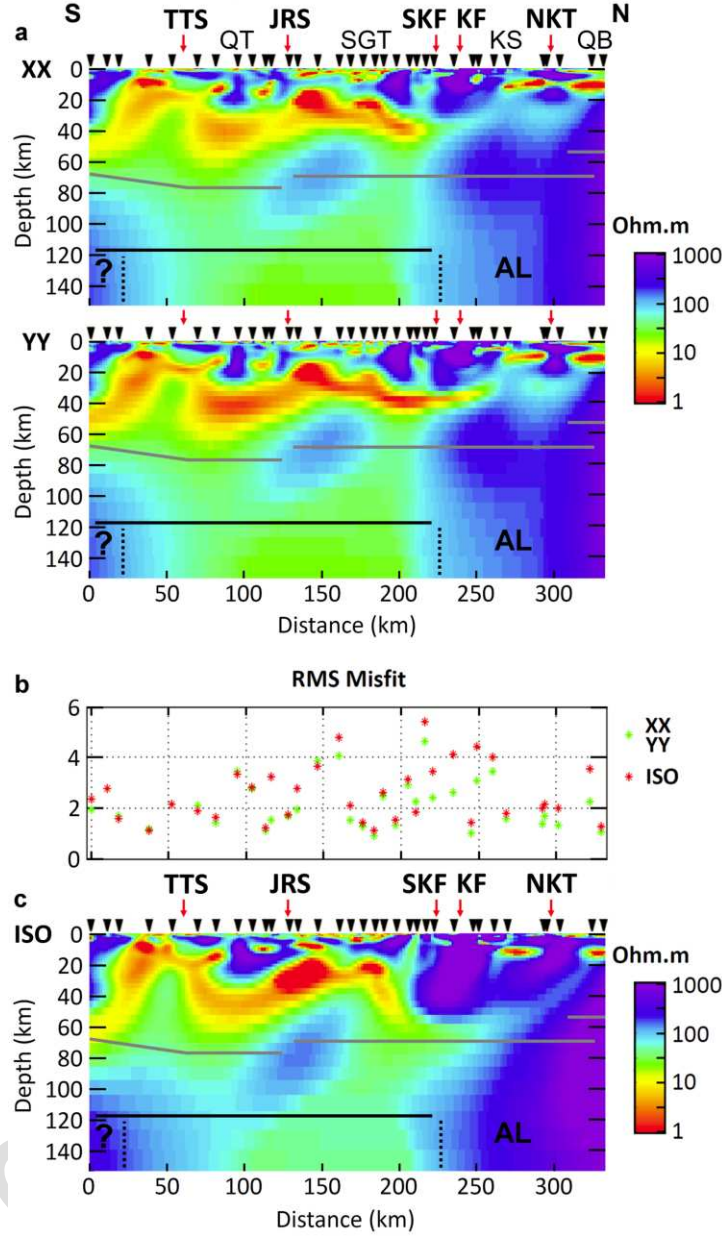
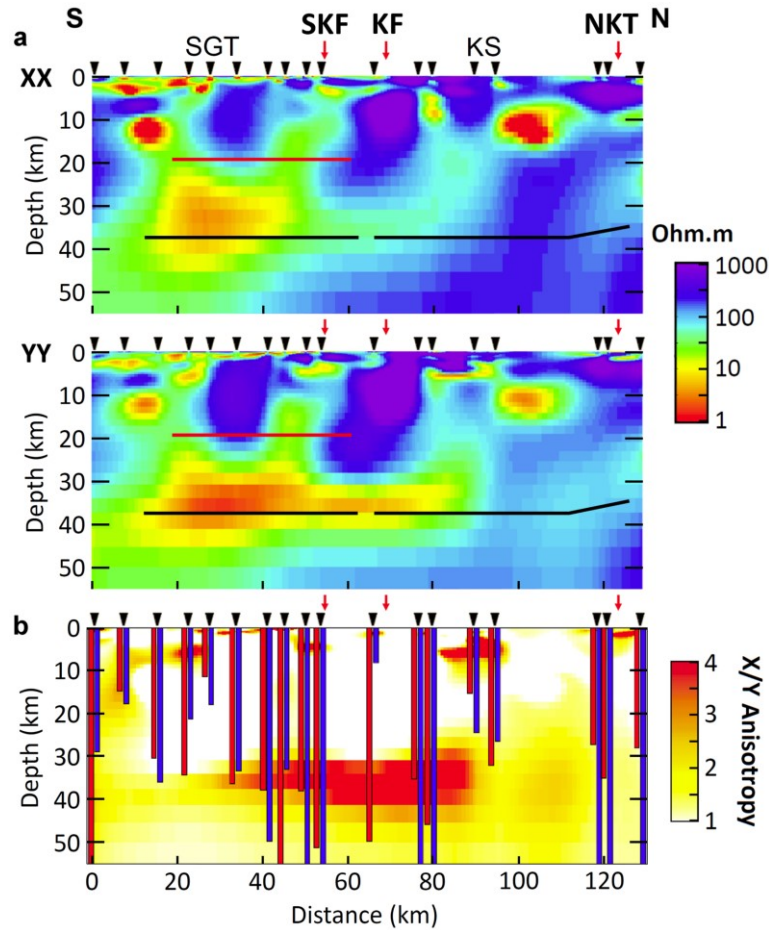


Figure 2. Global Anisotropic and Isotropic 2D Modelling. **a**, 2D anisotropic resistivity model. **b**, Difference between the anisotropic (green) and isotropic (red) RMS misfits. **c**, 2D isotropic resistivity model. For models **a** and **c**, the Moho depth^{21, 25} is highlighted by the grey line. The black line shows the LAB location for a thin Tibetan lithosphere in the north part of the plateau imaged by seismic receiver functions¹⁸. AL – Asian Lithosphere, QT – Qiangtang Terrane, SGT – Songpan-Ganzi Terrane, KS – Kunlun Shan, QB – Qaidam Basin.



290

291 **Figure 3. Local Crustal Anisotropic 2D Modelling. a**, 2D crustal anisotropic resistivity model.

292 Only periods lower than 1000s were considered for the crustal model. The final RMS of the

293 inversion is 1.94. Two seismic reflectors highlight the top (red) and the bottom (black) of a

294 relative low seismic velocity layer²⁵. **b**, Anisotropic differences between the xx and yy models.

295 It highlights the conductor extension observed in the yy model beneath the Kunlun Shan. The TE

296 (red) and TM (blue) modes approximate Niblett-Bostick penetration depth³⁰ are also shown on

297 plot **b**.

298

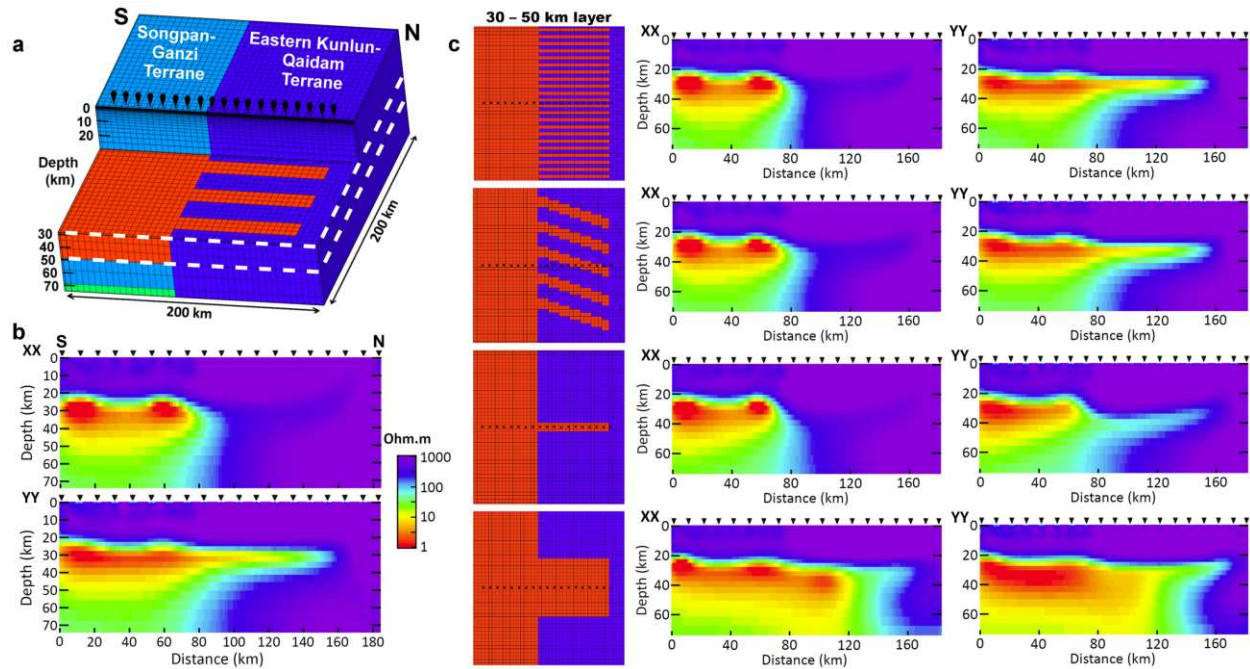


Figure 4. 3D synthetic modelling associated with 2D anisotropic inversion. a, 3D forward model (5x5 km horizontal gridding). The 3D synthetic data was generated for 19 stations using WinGLink²⁴ and random noise was added to the synthetic apparent resistivity (5%) and phase (1.5°) independently. **b**, 2D anisotropic inversion model associated with the model **a**. The synthetic data were inverted with the same 2D anisotropic inversion⁹ as the observed data. **c**, Four alternatives to the model **a** (only the 30-50 km layer differs) and the corresponding 2D anisotropic inversions.